

Article

Static and Fatigue Characterization of Adhesive T-Joints Involving Different Adherends

Georgino C. G. Serra ¹, José A. M. Ferreira ² and Paulo N. B. Reis ^{2,*}

¹ Department of Electromechanical Engineering, University of Beira Interior, 6201-001 Covilhã, Portugal; georgino.serra@sapo.pt

² University of Coimbra, CEMMPRE, ARISE, Department of Mechanical Engineering, 3030-788 Coimbra, Portugal; martins.ferreira@dem.uc.pt

* Correspondence: paulo.reis@dem.uc.pt

Abstract: It is very important to understand the damage mechanisms as well as the mechanical response of T-joints involving different materials on the base plate. For this purpose, two configurations were studied. In one, the joint is composed of a base plate and a T-element, both in Al 6063-T5, while in the other one, the aluminum base plate was replaced by a glass fiber composite. Finally, each configuration was divided into two batches, where in one, the elements were bonded with a stiff adhesive (Araldite® AV 4076-1/HY 4076) while in the other, a more ductile adhesive (Araldite® AW 106/HV 953 U) was used. The static and fatigue strength of all configurations was evaluated in bending. In all cases, the damage occurred at the end of the T-element, where a crack appeared and propagated toward the interior of the T-joint. The bending strength is highest for joints involving aluminum and the ductile adhesive, which is 2.8 times higher than the same configuration involving composite base plates and 1.7 times higher than that using the stiff adhesive. Finally, the highest fatigue lives were obtained for T-joints involving Al 6063-T5 base plates, and regardless of the base plate material, the ductile adhesive promoted the highest fatigue strength.

Keywords: structural adhesives; T-joints; static characterization; fatigue strength; damage mechanisms; mechanical testing



Citation: Serra, G.C.G.; Ferreira, J.A.M.; Reis, P.N.B. Static and Fatigue Characterization of Adhesive T-Joints Involving Different Adherends. *Processes* **2023**, *11*, 2640. <https://doi.org/10.3390/pr11092640>

Academic Editors: Hideki KITA and Raul D. S. G. Campilho

Received: 10 July 2023

Revised: 29 August 2023

Accepted: 31 August 2023

Published: 4 September 2023



Copyright: © 2023 by the authors. Licensee MDPI, Basel, Switzerland. This article is an open access article distributed under the terms and conditions of the Creative Commons Attribution (CC BY) license (<https://creativecommons.org/licenses/by/4.0/>).

1. Introduction

Compared to traditional joining methods (bolted, riveted or welded joints), adhesive joints have significant advantages due to the absence of fretting between materials, better fatigue response, and easier adaptation to complex shapes, among others. In addition to these advantages, adhesives are also increasingly reliable and durable. Therefore, it is not surprising that adhesive joints are increasingly being adopted by different industrial sectors [1].

In this context, and depending on the specific application or loading mode, designers have a wide variety of joint architectures at their disposal, where the single lap joints are the most used due to their simplicity and low cost [2,3]. However, they are responsible for promoting high shear and peeling stresses despite the various strategies that can be adopted to minimize them. Some examples include changing the strength and modulus of the adhesives and adherends [4–7], the thickness of adhesives and adherends [4–6], the overlap length [2,6], and adding fillets to the overlapped edges [8]. While these strategies increase the efficiency of single-lap joints, they cannot change the preferred loading mode for which they were designed. Therefore, to overcome this problem, T-joints are used to transfer bending, compressive, shear, and tensile loads between the leg panel and the base panel [9].

In terms of industrial applications, they can be used in the aircraft, automotive and marine sectors. In the first one, Johnson and Kardomateas [10] studied an adhesively bonded insert type T-joint for use in a composite space frame due to its high specific

stiffness and large bond area. In this study, a finite element analysis was performed to obtain the stress distribution along the joint. Regarding naval applications, the University of Southampton developed extensive work on T-joint design and performance in which, for example, Sheno and Violette [11] studied the influence of T-joint geometry on the ability to transfer out-of-plane loads in small boats. They concluded that geometry and material have a significant influence on the T-joint strength, but the radius of the fillet and the thickness of the overlamine are the most determining parameters. Finally, in terms of aeronautic applications, T-joints are very favorable due to their structural efficiency, simplicity, and lightness. In this context, Moreno et al. [12] proposed a system to take advantage of the energy that could be dissipated by the structural bonded joints.

However, complete knowledge of joint strength and damage mechanisms is required to allow widespread use. From the different studies available in the literature [13–16], it is possible to conclude that the failure initiates in regions where high stresses occur, so it is important to find these critical points for specific design solutions and geometric parameters. For example, Sheno and Hawkins [17] observed that although the geometry and material influence the strength and failure modes of T-joints, the fillet radius and the thickness of the overlamine are determining parameters. On the other hand, the gap between the panels and the edge preparation of the T-piece showed less expressiveness. According to Dodkins et al. [18], there are two critical variables for T-joints: the thickness of the overlamination and the fillet radius. While in the first case, its increase affects the performance of the joint, in the case of the fillet, it allows the joint to support higher loads. However, Sheno et al. [19] found that the influence of key variables is very dependent on the loading mode. Moreover, the effect of geometric parameters on stiffness, strength, and failure region is also significantly dependent on loading mode [15,16,20]. Finally, Chaves et al. [21] compared the strength of adhesive T-joints with screwed ones and observed that the adhesive joints have a similar or better mechanical performance than conventional screwed T-joints. However, they also noted that the strength of adhesive T-joints could be further improved by using spew fillets at the ends of the overlap.

According to Zhan et al. [22], the joint's dimensions, the size of the adherend and adhesive bondline, as well as the mechanical properties of the constituents (adherend and adhesive) significantly affect the strength of the T-joints. Therefore, based on these considerations, they studied experimentally and numerically the effect of different geometries subjected to a tensile load, concluding that the geometry of the bondline has a strong effect on the stress distributions, stress concentrations, and load-bearing capacity. Furthermore, it was also observed that the displacement of the Y axis tends to decrease with the increase in the average bondline area, while the average failure load increases with the increase in the average bonding area. Finally, the asymmetry of the stringer can cause unequal Von Mises equivalent stress distributions, higher Von Mises equivalent stresses, and deflection deformations. Ferreira et al. [23], using the finite element method (FEM) and cohesive zone models (CZM), studied the mechanical performance of different T-stiffener configurations under peel loads. For this purpose, authors considered the following geometrical parameters: flat adherend thickness (t_p), stiffener thickness (t_0), overlap length (L_0), and curved deltoid radius (R). They found a significant effect of all the parameters on both the stress distribution and maximum load. For example, the maximum load increased by around 94.1% when t_p was increased from 1 to 4 mm, decreased by about 27.3% when t_0 changed from 0.5 mm to 2.5 mm, increased by around 94.1% when L_0 was increased from 10 to 20 mm, and increased by around 135.4% when R was increased from 1 to 3 mm.

In T-joints, the stiffener can be a single part or composed of two L-shaped elements joined by co-curing or a structural adhesive. Using the last configuration (two L-shaped elements), Ma et al. [24] numerically (using the extended finite element method combined with cohesive zone model) and experimentally studied the damage mechanisms of carbon fiber reinforced polymer (CFRP) T-stiffeners subjected to pull-off loads. Contrary to what is reported in the literature, in which the final failure begins with the debonding in the radius region and then spreads to the stringer-skin interface, these authors observed a crack that

begins in the filler region and near the fillet apex due to the stress concentration in this region. Subsequently, the crack propagates vertically, generating a debonding between the two L-shaped elements (stringer/stringer) but also towards the skin. Finally, when the crack reaches the skin, it promotes debonding at the stringer-skin interface, which moves towards both ends until the final rupture. The authors also found that the crack in the filler region started at the location of the maximum principal strain and that the large strain concentration region was limited to the filler region and the composite laminates. Therefore, improving the mechanical performance of T-joints can be achieved by reducing the stress concentration at the critical points of the joint and/or distributing the stresses more evenly along the bondline, among other solutions reported by Ravindran et al. [25]. In the first case, for example, Carvalho et al. [26] proposed the dual-adhesive joining technique, in which flexible adhesives are used in regions of high stress and stiff adhesives in regions of low stress. Different adhesive ratios were considered, namely 12.5/75/12.5 mm and 33.3/33.3/33.3 mm, and a numerical study was developed using the CZM technique (cohesive zone modeling) in the ABAQUS[®] software (ABAQUS 2017, Dassault Systèmes, RI, USA). These authors observed that failure occurred at the bondline and in the transition zone between adhesives, with the maximum load not only changing position but also decreasing in magnitude. In this context, improvements in the strength of the T-joints were obtained compared to those using only one adhesive, although more significant for the 33.3/33.3/33.3 mm ratio. With regard to the more uniform distribution of stresses along the bondline, Morano et al. [27] very recently suggested an alternative approach that does not compromise the integrity of the skin and is based on the use of corrugated stiffeners. Compared to the conventional configuration (flat stiffeners), the corrugated ones promoted improvements of around 65% in terms of pull-out strength and about 416% for the absorbed energy. The authors observed that the modified stiffeners promoted a redistribution of the stress along the bondline, with a consequent reduction in peak stresses at the free edge.

In terms of fatigue life, literature does not present many studies on this subject. Shenoj et al. [9], for example, noted that for higher load values, the fatigue strength significantly depends on the fillet radius (larger radii promote longer fatigue lives), but when the load decreases, this effect is lost, and the fatigue strength decreases in both cases to a fatigue threshold. The damage accumulation was assessed in terms of global stiffness loss, and three different regimes were observed. Initially, the stiffness decreased very rapidly during the first 20% of the fatigue life, followed by an almost linear regime up to 80% of the fatigue life, after which a very rapid degradation occurred again until the final collapse. In another study, Read and Shenoj [28] observed that the fatigue life increases both with the increase of the fillet radius if the overlamine thickness (number of layers) is kept constant and with the increase of the overlamine thickness if the fillet radius remains constant. Studies developed by Marcadon et al. [29] showed that fatigue life is strongly influenced by frequency due to the viscous behavior of the different materials, especially for higher load levels. Loureiro et al. [30] studied T-joints and compared the fatigue strength of two different adhesives (an epoxy adhesive and a polyurethane adhesive). They observed that the slope of both fatigue curves and the dispersion of the data are very similar. Although elastomeric adhesives have better fatigue behavior, this phenomenon was explained by heating the adhesive during the fatigue tests (greater for the elastomeric adhesive than for the epoxy). Finally, more recently, Cullinan et al. [31] studied T-joints repaired by cyanoacrylate adhesive systems and found that the fatigue life was lower than that obtained in control (unrepaired) samples.

Therefore, from the available literature, it is very important to understand the damage mechanisms and the mechanical response of adhesive T-joints to expand their application in the most diverse industrial sectors. If this subject is already reasonably understood for static loads, in terms of fatigue life, it is still limited to a very small number of studies, which does not allow for well-consolidated knowledge. For this purpose, the present study intends to analyze the fatigue performance of adhesive T-joints involving aluminum adherends and adherends that combine aluminum and glass fiber-reinforced composites.

2. Materials and Methods

Figure 1 shows the T-joint geometry and respective dimensions used in this study. The first configuration analyzed used only aluminum elements and, for this purpose, $150 \times 30 \times 3 \text{ mm}^3$ Al 6063-T5 bars (Supplied by Alu-Stock, Madrid, Spain) were used as the base plate and T-elements of Al 6063-T5 with $30 \times 30 \times 2 \text{ mm}^3$ as the stiffener. The nominal chemical composition and average tensile properties of this alloy are summarized in Tables 1 and 2, respectively.

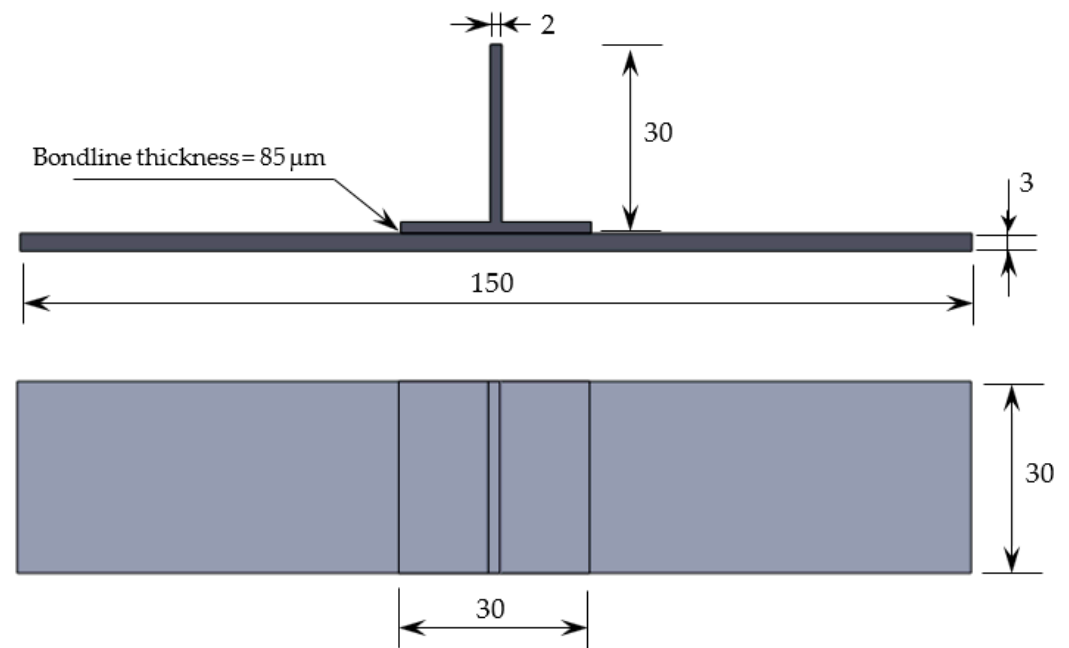


Figure 1. T-joint geometry and respective dimensions (in mm).

Table 1. Chemical composition (wt.%) of aluminum alloy 6063-T5 [32].

Si	Fe	Cu	Mn	Mg	Cr	Zn	Ti	Al
0.3–0.6	0.35	0.1	0.1	0.4–0.85	0.1	0.1	0.1	>96.9

Table 2. Principal mechanical properties of aluminum alloy 6063-T5 [32].

Elastic Limit (MPa)	UTS (MPa)	Elongation (%)	Young Modulus (GPa)	Hardness Brinell
145	187	≈12	68.9	60

The second configuration used composites in the base plates and stiffeners similar to the first configuration. Composite laminates were previously produced by hand lay-up using a Sicomin SR 8100 epoxy resin with SD 8824 hardener (both supplied by Sicomin, Chateaufeuf les Martigues, France) and eighteen layers of bidirectional glass fiber fabric (taffeta with 195 g/m^2). Details regarding the mechanical/physical properties of the resin and manufacturing process can be found in [33]. Finally, the $150 \times 30 \times 3 \text{ mm}^3$ base plates were cut from $330 \times 330 \times 3 \text{ mm}^3$ composite plates. The maximum error observed in the thickness of the base plates was 0.35 mm for the composite ones and 0.04 mm for the aluminum ones.

Subsequently, two batches of samples were produced. In one of them, the base plates and T-stiffeners were bonded with the adhesive “Araldite® (Lausanne, Suisse) AV 4076–1 resin/HY 4076 hardener”, while in the other one, the adhesive “Araldite® AW 106 resin/HV 953 U hardener” was used. The main mechanical properties of these

adhesives are reported in [34,35]. These two-part paste adhesives were selected because the first one (Araldite® AV 4076-1/HY 4076) is a very stiff and brittle epoxy, and the last one (Araldite® AW 106/HV 953 U) is flexible/ductile. Before bonding, all surfaces to be joined (both base plates and T-stiffeners) were abrasively prepared with P220 silicon carbide paper and then cleaned with dry air and alcohol. This methodology was successfully applied in several previous studies [2,36–39], where the passive mechanical method used does not actively alter the chemical nature of the surface but only cleans the substrate and removes weak boundary layers in the form of contamination. Finally, to ensure a constant bondline thickness, all specimens were subjected to constant pressure during the adhesive curing process, and for this purpose, black metal dovetail clips were used. As reported in Figure 2 (a representative roughness profile), a pressure of 0.11 MPa applied to the specimens leads to an average bondline thickness of 85 μm without significant dispersion. Based on studies available in the literature [39–41], this value was obtained/measured after testing using a Mitutoyo (Kawasaki, Japan) SURFTEST SJ-500 surface measuring system.

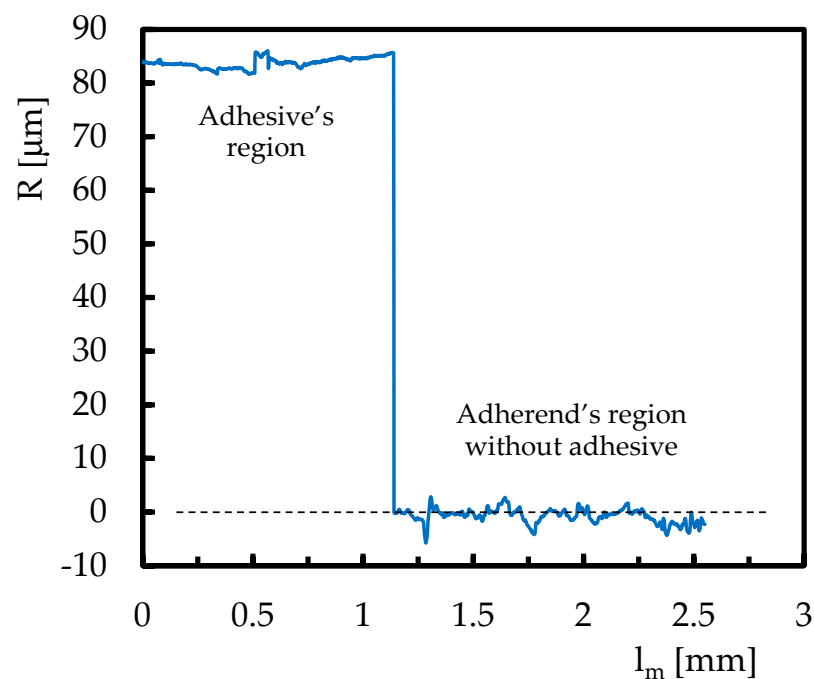


Figure 2. Typical roughness profile (R = roughness size; l_m = evaluated length).

The curing process was carried out at 40 °C for 16 h. According to Serra et al. [42], these parameters do not maximize the mechanical properties of the adhesives, but they were the most appropriate considering the T_g (glass transition temperature) of the resin used in the composite laminates. Therefore, for comparability of results between specimens with different base plates, a temperature of 40 °C was used for all batches analyzed.

These specimens are used to study the effect of materials (at the level of base plates) and adhesive type on the mechanical performance of T-joints. For this purpose, static three-point bending (3PB) tests are carried out at room temperature on a Shimadzu universal testing machine, model Autograph AGS-X (Shimadzu, Kyoto, Japan), equipped with a 100 kN load cell. As can be seen in Figure 3, the span used in the 3PB tests was 100 mm, with a displacement rate of 5 mm/min, and for each condition, three specimens were tested. Regarding the fatigue tests, they were carried out in an E 10000 Instron Electropulse (Norwood, MA, USA) uniaxial fatigue testing machine equipped with a 10 kN load cell and controlled by a computer with data acquisition. These tests were performed at room temperature, under a constant amplitude sinusoidal waveform loading, a stress ratio (R) of 0.05, and a frequency of 10 Hz. The load levels used in this study were selected to obtain fatigue lives between 10^3 and 10^6 cycles, and similar to the static tests, the load

was also applied according to the schematic representation shown in Figure 3. Finally, the failure surface morphologies were also analyzed in detail using different techniques and equipment, such as a Mitutoyo SURFTTEST SJ-500 surface measuring system, a Hirox (Hackensack, NJ, USA) RH 2000 microscope, and a Hitachi (Tokyo, Japan) Scanning Electron Microscopes SU3800.

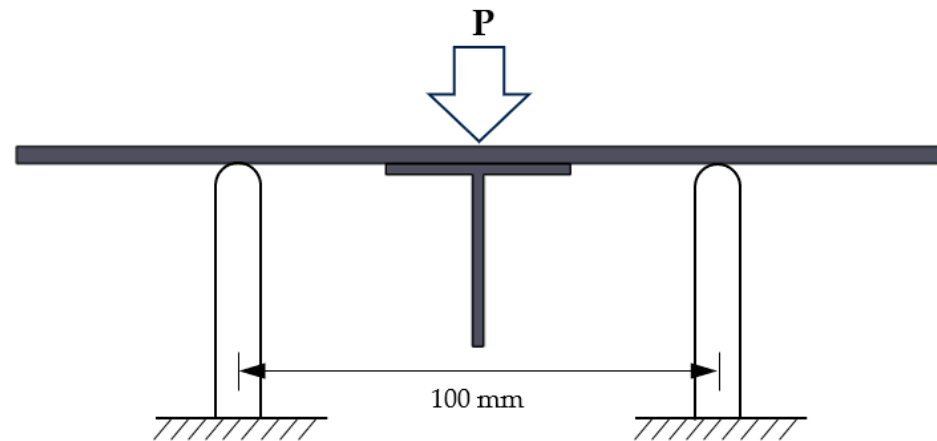


Figure 3. Apparatus and load mode used in static and fatigue testing.

3. Results and Discussion

The static response of the different T-joints was analyzed by 3PB tests according to Figure 3, and the results are shown in Figure 4. As reported by Loureiro et al. [30], due to non-uniform shear stresses and significant peel stresses that occur in this geometry, it is preferable to indicate the load rather than the stress. Therefore, this analysis avoids extremely misleading average shear stresses.

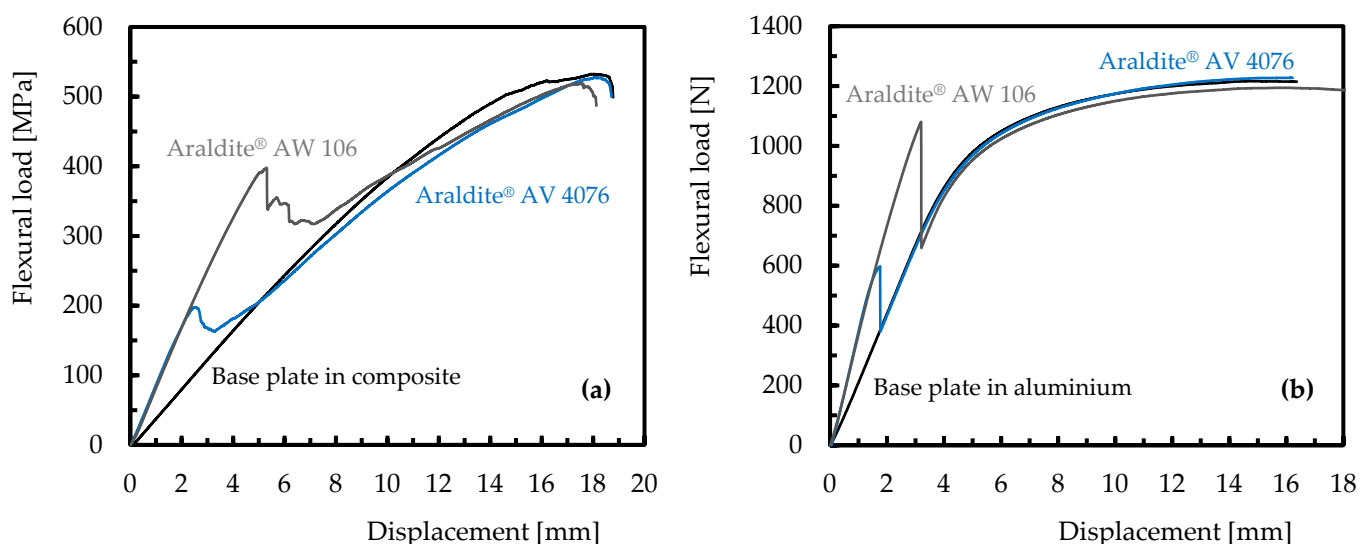


Figure 4. Flexural load-displacement curves for (a) T-joints involving base plates in the composite and (b) T-joints involving base plates in aluminum.

It is possible to observe that, for all the configurations studied (involving different base plate materials and adhesive types), the load increases linearly up to a maximum value, from which it starts to decrease until it reaches values close to those of the load displacement curve of the base plate material. Subsequently, the load-displacement curves practically overlap those of the base plates. It is also noticeable that the first peak load strongly depends on the adhesive type used in the T-joints as well as the material of the base plates. In fact, ductile adhesives can deform plastically and provide higher elongations

than brittle adhesives before their collapse. Consequently, the highest peak loads observed for the ductile adhesive can be explained by the lower stress concentrations at the ends of the adhesive edges and better redistribution of stresses as the load increases [43,44]. On the other hand, regardless of the adhesive, peak loads are higher for T-joints involving Al 6063-T5 base plates because a higher stiffness of the adherends promotes a more uniform distribution of stresses in the adhesive [7]. In this context, the material that is less stiff determines the strength of the joint [7], and different failure mechanisms can be expected. Finally, for both adhesives, the second peak load is strictly related to the maximum load value observed for the base material. After the second peak load, the load always decreases more or less rapidly depending on the type of base material.

From Figure 4, it is also possible to obtain the main static properties, which are summarized in Table 3 in terms of average values and respective standard deviation. Stiffness was defined as the slope in the linear region of the load-displacement response, and the displacements are the values obtained for the different peak loads.

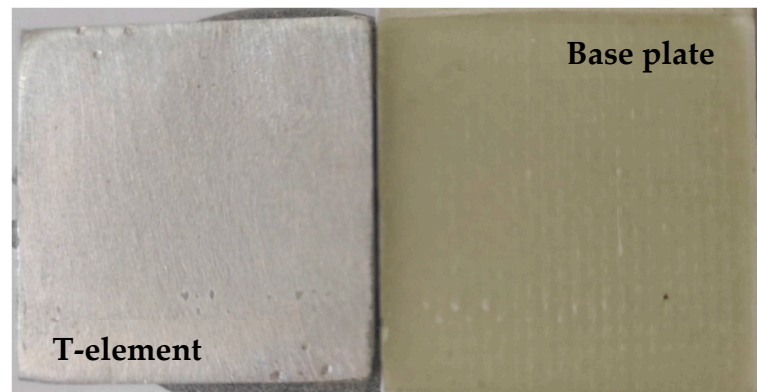
Table 3. Main static properties obtained for the different T-joints studied.

Base Plate Material	Adhesive	First Peak			Second Peak	
		Load [N]	Disp. [mm]	Stiffness [N/mm]	Load [kN]	Disp. [mm]
Composite plate	-	498.7 (± 49.8)	18.1 (± 2.31)	43.8 (± 5.3)	-	-
Al 6063-T5 plate	-	1213 (± 11.0)	15.6 (± 0.20)	225.7 (± 2.0)	-	-
Composite	AW 106	389.6 (± 7.3)	5.8 (± 0.49)	79.5 (± 4.5)	519.1 (± 50.5)	17.5 (± 0.85)
	AV 4076-1	228.6 (± 7.4)	3.5 (± 0.14)	79.4 (± 10.4)	491.8 (± 49.8)	18.8 (± 0.82)
Al 6063-T5	AW 106	1080.1 (± 65.5)	3.6 (± 0.51)	386.3 (± 13.2)	1204.5 (± 32.8)	15.8 (± 0.20)
	AV 4076-1	626.7 (± 25.2)	1.9 (± 0.13)	399.6 (± 6.3)	1200.9 (± 22.3)	15.5 (± 0.55)

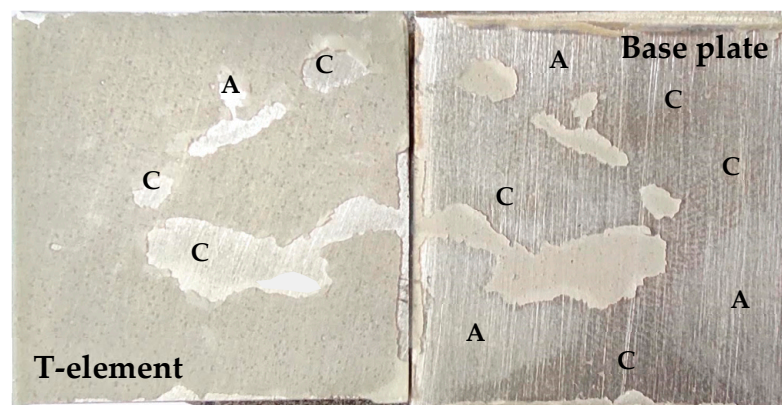
(\pm SD)—Standard deviation values.

It is possible to observe that Al 6063-T5 base plates have the highest maximum load (about 2.4 times higher) and stiffness (about 5.1 times higher) and the lowest displacement at maximum load (about 13.8% lower) compared to the values obtained for the composite base plates. Regarding the adhesive joints, and regardless of the adhesive used, it is clearly noticeable that the second peak of load practically coincides with the maximum load value observed for each type of material used in the base plate. The dispersion is very small and, as can be seen in the results and in Figure 3, after a certain value, the curves of the base materials almost overlap with those of the T-joints. Finally, the effect of the T-element on the mechanical performance of the adhesive joints is significant only up to the first peak, proving to be dependent on the base plate material and type of adhesive used, after which the joint strength is similar to that of the base plate. The highest load peaks are obtained with the ductile adhesive (AW 106), where the values obtained for T-joints involving Al 6063-T5 base plates are 2.8 times greater than those involving composite base plates. On the other hand, the opposite is observed for displacement, where the maximum values are 1.6 times greater for T-joints involving composite base plates. However, comparing the adhesive type for joints with composite base plates, the ductile one accounts for 70.4% higher peak loads, while in terms of displacement, it is around 65.7%. For joints with Al 6063-T5 base plates, these values are 72.3% and 89.5% respectively. Lastly, regardless of the adhesive type and base plate material, it is quite evident that the bending stiffness values of the T-joints are much higher than those observed for the base plates (81.5% for composites and 74.1% for Al 6063-T5) due to the reinforcing effect introduced by the T-element, but very similar to each other despite the adhesives being different. For example, for T-joints involving composite base plates, the average bending stiffness is around 79.5 N/mm, while for those involving Al 6063-T5, it is about 393 N/mm. In the last case (T-joints involving Al 6063-T5 base plates), the stiff adhesive promotes a small difference of 3.3% in relation to the ductile one, but this value is statistically insignificant in relation to the observed

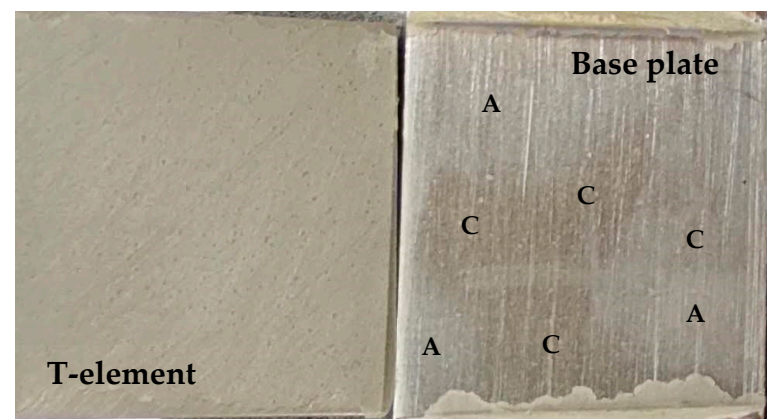
dispersion. Therefore, the stiffness introduced by the T-element is clearly more important than the effect of the adhesive type, which would be expected given the bondline thickness. To complement the results described above, the failure surface morphologies were also analyzed and are shown in Figure 5.



(a)



(b)



(c)

Figure 5. Typical failure morphologies for T-joints involving: (a) Composite base plates and ductile adhesive; (b) Al 6063-T5 base plates and ductile adhesive; (c) Al 6063-T5 base plates and stiff adhesive. (A = adhesive failure, C = cohesive failure).

A first analysis of Figure 5 shows that there are two failure modes, one for T-joints with composite base plates and another for those involving Al 6063-T5 base plates. In the first case, although Figure 5a shows only the damage morphology for T-joints with ductile adhesive, it is also representative of those involving the stiff adhesive. Therefore, for these joints, the failure is typically adhesive, with all the adhesive (whether ductile or stiff) remaining in the T-element (see Figure 5a). On the other hand, all T-joints involving Al 6063-T5 base plates revealed a mixed adhesive/cohesive failure mode (see Figure 5b,c). Adhesive failure (represented in Figure 5 by the letter “A”) occurs when the forces exerted on the joint are greater than those between the adherend and adhesive, while cohesive failures (represented in Figure 5 by the letter “C”) occur when the bond between molecules within the adhesive fails due to the greater external force. In this context, cohesive failure occurs when the maximum adhesive strain exceeds its limit [45].

To confirm the occurrence of mixed adhesive/cohesive failure mode, the authors used different techniques to assess the damage in different failure regions. Figure 6, for example, shows the roughness profile along a line (L) covering different failure modes and for a T-joint involving the Al 6063-T5 base plate and the ductile adhesive (Figure 5b). From the roughness profile shown in Figure 6, it is possible to identify three distinct regions: Region 1, which corresponds to an adhesive failure but with the adhesive layer completely on the T-element; Region 2, where the adhesive failure is also identified but with the adhesive layer completely over the base plate; and Region 3 where a cohesive failure occurs. In this case, a part of the adhesive remains on the T-element (about one-third of the thickness) and the rest on the base plate (the remaining two-thirds). As reported above, this defect is due to the strain having exceeded the maximum strain of the adhesive or, in other words, the external force is greater than the internal forces between molecules of the adhesive [45].

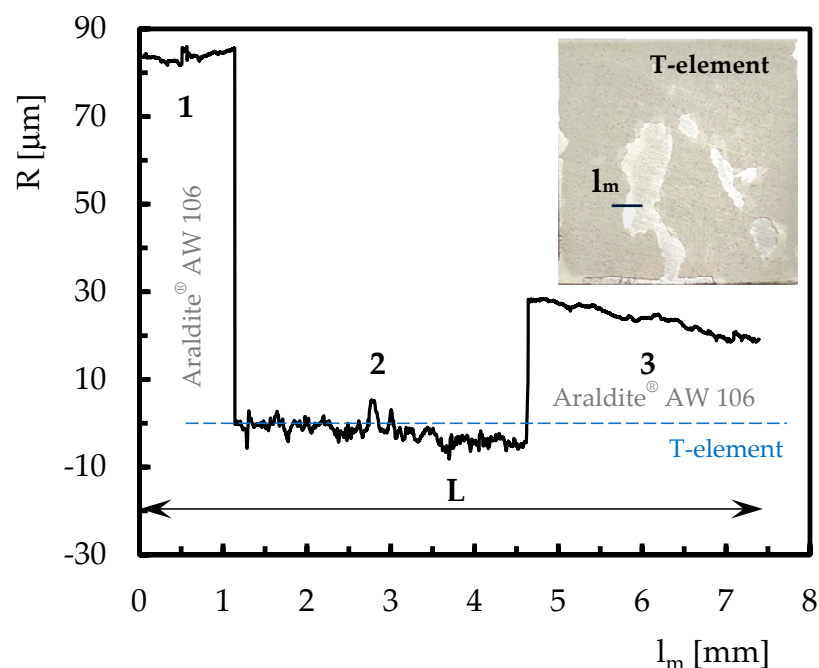


Figure 6. Roughness profile along the indicated line (l_m) for a T-joint involving aluminum base plate and ductile adhesive (R = roughness size; l_m = evaluated length).

Subsequently, because Figure 5b,c shows darker regions, especially at the level of base plates, they were analyzed to determine what type of damage would be underlying them. In this context, Figure 7 shows the analysis developed by digital microscopy (Hirox RH 2000 microscope) of a T-joint involving the Al 6063-T5 base plate and the stiff adhesive (Figure 5b), where it is evident that the darker regions are very thin films of adhesive.

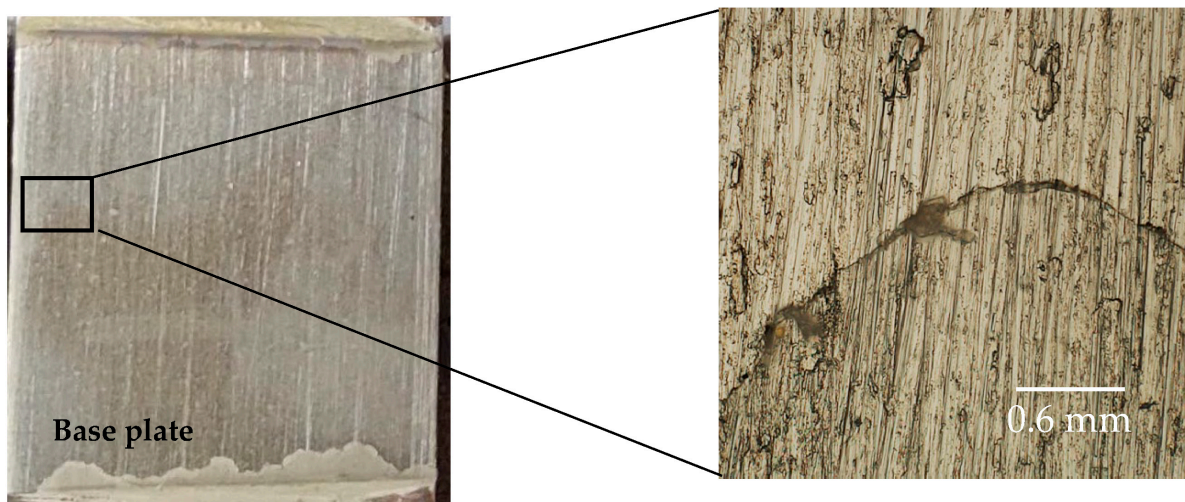


Figure 7. Analysis developed by digital microscopy of a T-joint involving the Al 6063-T5 base plate and the stiff adhesive.

Although this technique is not as informative as the previous one because it does not allow thicknesses to be assessed, it clearly shows the existence of a thin film of adhesive on the base plate, with the remainder on the other adherend (i.e., adhered to the T-element). In this context, despite its simplicity, it proved the presence of adhesive traces in the adherend and, consequently, the existence of a cohesive failure. However, to deepen this analysis even further, scanning electron microscopy (SEM) and energy dispersive X-ray spectroscopy (EDS) were used to obtain more precise and magnified images of the fracture surface, as well as to identify its elemental chemical composition. Figure 8 shows, in this case, the results obtained from the SEM/EDS analysis for a specific region of Figure 5b.

This region A was selected because it apparently represents an adhesive failure, with one part of the adhesive on the base plate and the other part on the T-element. However, in detail, Figure 8a shows the existence of two regions, where the darker one represents the adhesive while the lighter one represents the surface of the T-element with eventual traces of adhesive. To prove this evidence, Figure 8b shows the analysis of the elemental chemical composition carried out along area A represented in Figure 8a. From this figure (Figure 8b), it can be observed that the darker region of Figure 8a is essentially constituted by hydrogen (H) and oxygen (O), chemical elements typical of the adhesive, while the lighter one is dominated by Al (aluminum), an element that underlies the chemical composition of the 6063-T5 aluminum alloy (>96.9%, according to Table 1) of the T-element. In addition to this chemical element, (Al), H (hydrogen), and O (oxygen) are also present, which confirms the presence of adhesive traces on the surface of the T-element. This evidence proves that an optical microscopy analysis similar to that carried out in Figure 7, based on light and a combination of lenses to magnify an image, is not entirely effective for assessing failure modes in adhesive joints. In fact, it does not allow for detection with complete assertiveness of the existence of adhesive traces on fracture surfaces because many of them can be confused with roughness or other defects in the adherends (see Figures 7 and 8a,b). Therefore, what initially appeared to be an adhesive failure region, this technique showed the existence of adhesive traces, changing the failure mode to mixed but with a larger predominance of the adhesive mode. On the other hand, when compared with the roughness analysis that supports Figure 6, the latter also does not clarify that in regions 1 and 2, there are adhesive traces on both adherends. Consequently, this technique should be used together with SEM/EDS to have a complete analysis of the damage mechanism. Finally, Figure 8c shows the elemental chemical composition between two points and along a trajectory (points 1 to 2 shown in Figure 8b). It can be seen that point 1 is on the adhesive due to the strong predominance of carbon (C), and point 2 is on the adherend where Al (aluminum) predominates, confirming the analysis reported above.

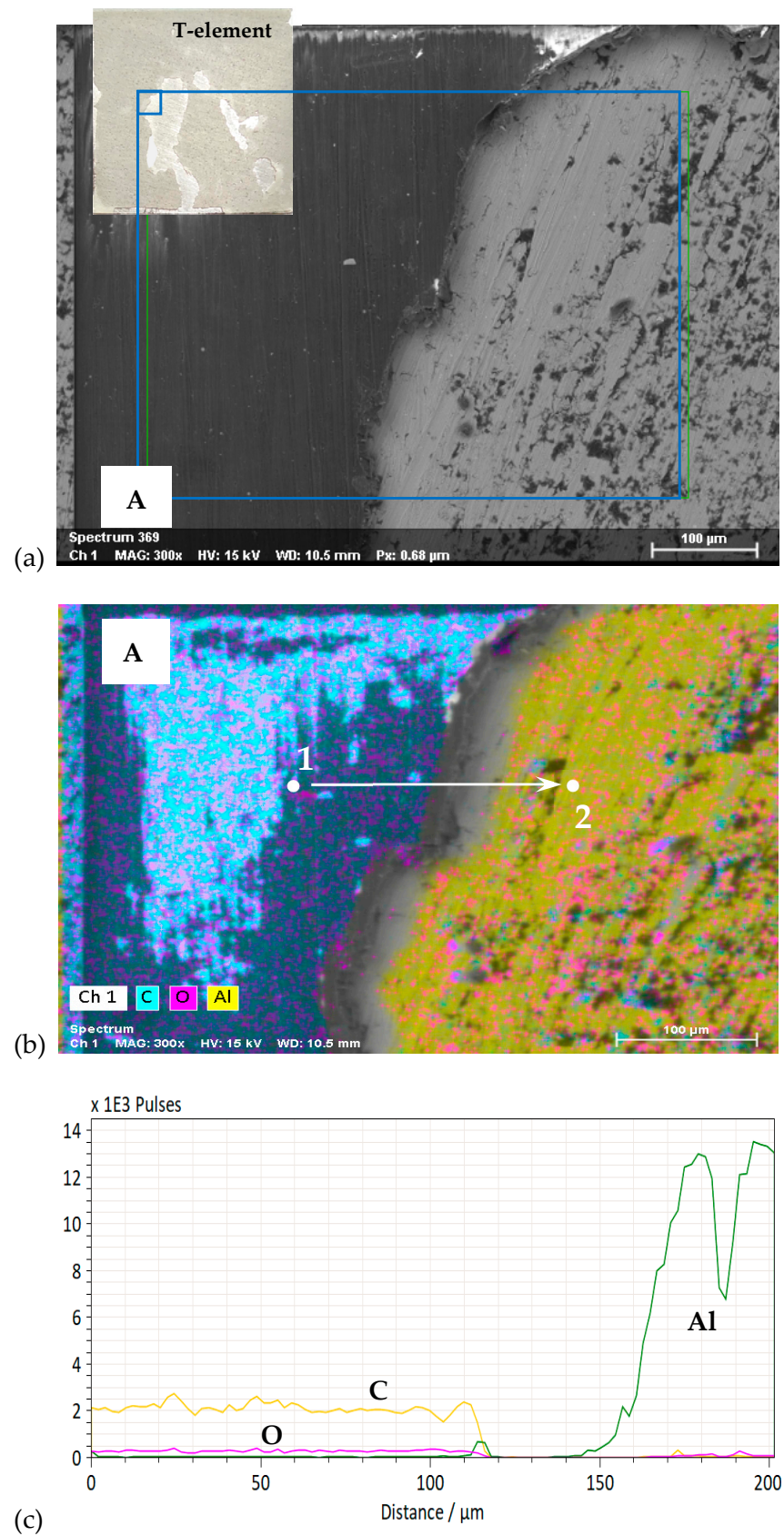


Figure 8. SEM-EDS analysis showing: (a) Fracture surface; (b) elemental chemical composition map; (c) distribution of elemental chemical composition between two points.

Based on the representativeness of the failure modes presented in Figure 5 and the various techniques that promoted the discussion supported by Figures 6–8, the areas related to the adhesive and cohesive failures were obtained using the ImageJ software (a graphic design tool dedicated to analyzing images). From this assessment, it was possible to observe that while in T-joints with the ductile adhesive, the cohesive area represents about 48.3% of the total bonded area, this value is only 3.8% lower for those involving the stiff adhesive. Another piece of evidence that can be taken from this study is the fact that adhesion between adhesives and aluminum is higher than between adhesives and composite. In fact, it would be possible to increase the adhesion using the various surface treatments suggested in the literature, but the authors chose not to adopt them in order to bring the study as close as possible to the reality of some industries where assemblies are made along the production line and from a mass production perspective [46]. However, according to Loureiro et al. [30], these conditions promote a higher scatter of failure loads.

To conclude this study and understand the typical profile of the curves shown in Figure 4, the bending tests were monitored by a high-speed video camera to assess the damage as a function of load. Figure 9 shows some damages for specific load values, and although the image sequence was obtained for a T-joint involving only aluminum and the stiff adhesive, it is representative of all other configurations. Therefore, based on the repeatability observed for all configurations, it can be noted that the load increases almost linearly up to a certain value that depends on the base plate material and the adhesive used (representative point—A). Subsequently, when the load reaches its first maximum (B), a crack appears at the end of the T-element between the adhesive and adherend (adhesive failure) or within the adhesive (cohesive failure). As reported above, adhesive failure occurs when the forces exerted on the joint are greater than those between adherend/adhesive, and cohesive failures occur when the maximum adhesive strain exceeds its limit [37]. Subsequently, after the first load peak (B), the load decreases more or less abruptly due to the propagation of the crack towards the interior of the reinforcement element until it reaches a value that coincides with the load-displacement curve of the base plate (D). For this load value (D), the damage has already reached half the length of the T-element. Thereafter, the damage propagation is negligible, and the load-displacement curves of the T-joints practically overlap with those of the base plate material (E). In this case, the load increases until it reaches a second peak load, which coincides with the maximum load of the base plate material. Therefore, for this geometry and loading, the structural integrity of the T-joints as a whole is only guaranteed up to the first peak load, after which it is ensured only by the base plate.

These results are in line with those observed by Hirulkar et al. [47], where the same behavior (significant load drop) was observed and explained by the appearance of cracks at the end of the overlap. Compared to the in-plane loading, the bending that is imposed here is responsible for a significant deflection in the joint, and consequently, higher peel stress concentrations occur [48,49]. In this case, the simultaneous action of tensile peel and shear stresses is responsible for the first cracks that appear at the end of the T-element (B) [42,50].

Regarding the fatigue response of the different T-joints, the results are shown in Figure 10 in terms of load versus the number of cycles to failure on a logarithmic scale for both adhesives and materials. The typical representation for a fatigue analysis (SN curves) was adopted, but instead of stress, loading was implemented due to the non-uniform nature of shear stresses and the existence of significant debonding stresses in these joints [30]. As already mentioned, these results were obtained for different constant amplitude loads, whose values were selected to obtain fatigue lives between 10^3 and 10^6 cycles. Moreover, it was ensured that all of them were lower than the first peak load observed in the static curves (Table 3) to guarantee the structural integrity of the adhesive joints at the beginning of each test and the existence of a load value common to all configurations for comparability of the results (in this case 150 N). Based on the static analysis performed around Figure 9 (damage initiation and its propagation), the fatigue failure criterion adopted considered the instant when the crack reaches half the length of the T-element (see Figure 9). However,

because this methodology incorporates some subjectivity or the crack front may not be detectable by optical methods, it was necessary to adopt a more accurate methodology. Therefore, from the results collected by the data acquisition system, it is possible to plot, for example, the maximum load versus number of cycles and the maximum displacement versus number of cycles curves, as shown in Figure 10a. Although these curves were obtained for the T-joint involving Al 6063-T5 base plates, the ductile adhesive (AW 106), and a maximum load of 350 N, they are representative of all the others.

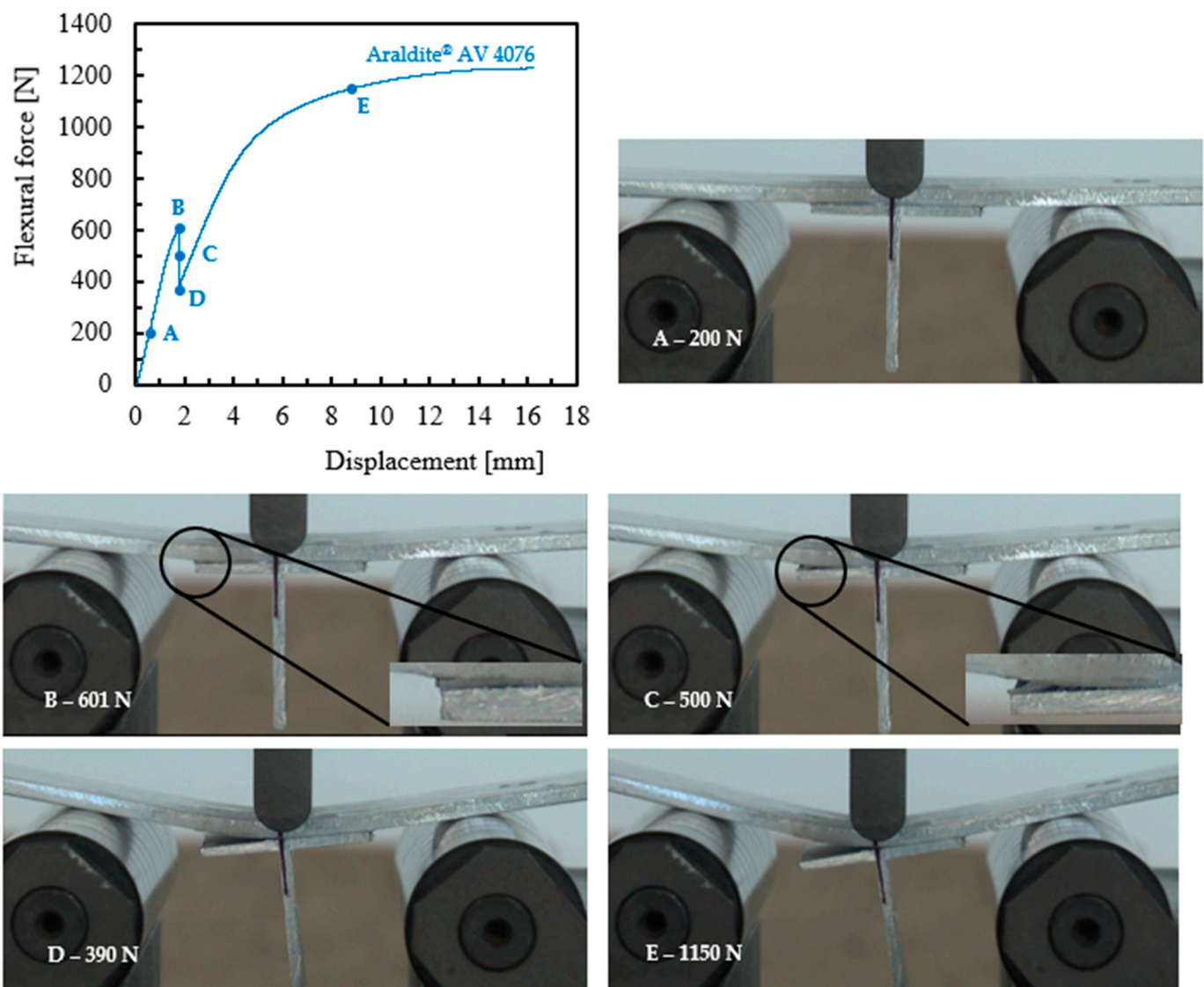


Figure 9. Damage evolution observed for T-joints involving only aluminum and a stiff adhesive.

In this context, because the load is constant, the fatigue failure criterion considers the number of cycles obtained for the first plateau point (N_f), from which the displacement is controlled by the stiffness of the base plate. Consequently, based on this methodology, the load versus number of cycles curves for the different configurations are shown in Figure 10b,c, where the mean curve fitted to the experimental results is also superimposed.

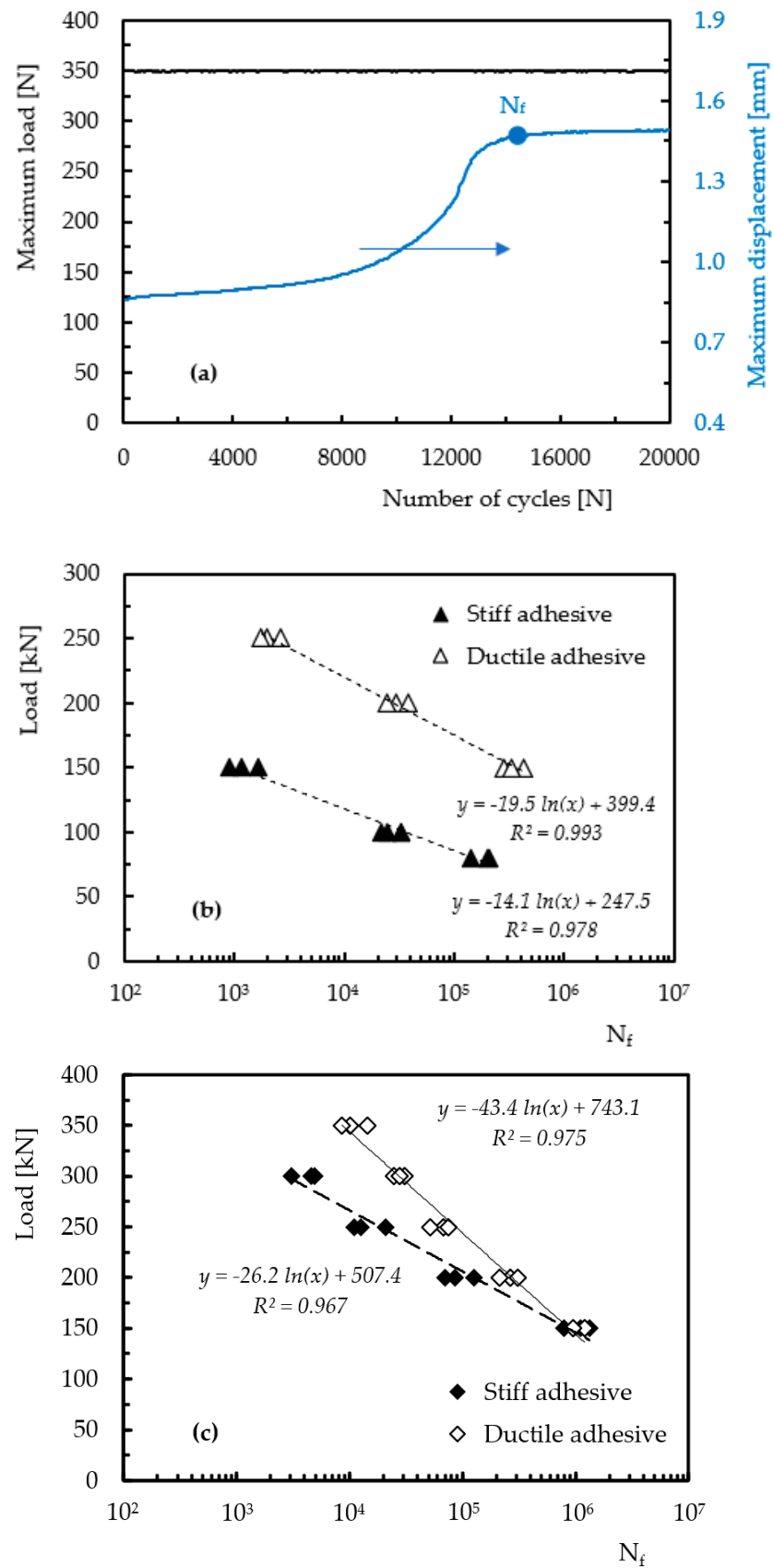


Figure 10. (a) Maximum load versus the number of cycles and maximum displacement versus the number of cycles; (b) fatigue life curves for T-joints involving composite base plates; (c) fatigue life curves for T-joints involving aluminum base plates.

From these figures, it is possible to observe that, when comparing T-joints involving composite base plates and the same load value (150 N), the ductile adhesive (AW 106) promotes fatigue lives about 280 times longer than those observed for the stiff adhesive (AV 4076–1). The slope of the fatigue curves shows some convergence for very long lives (Figure 10b), although T-joints involving the ductile adhesive always denote higher fatigue strength. On the other hand, regarding the T-joints involving Al 6063-T5 base plates (Figure 10c), it is noted that the curves converge for the 150 N load and with very close fatigue lives, i.e., the adhesive type has no effect on the fatigue strength for this load level. This behavior is very similar to that noticed for T-joints involving composite base plates, but with much greater convergence and fatigue lives about 871 and 3 times longer than those observed with brittle and ductile adhesive, respectively. Furthermore, increasing the load leads to greater differences in fatigue lives between the T-joints with the different adhesives used, reaching around 6.6 times for the 300 N load (see Figure 10c). Therefore, it is evident from Figure 10b,c that the ductile adhesive is responsible for longer fatigue lives due to higher percentages of elongation before failure and lower stress concentrations [43,51].

According to the bibliography, stiff adhesives experience higher stress concentrations and early failure compared to ductile ones [43]. For example, Temiz [52] observed that the use of ductile adhesives decreases the stress concentrations at the overlap ends and, consequently, increases the strength as well as delays the beginning of the failure due to their high strain to failure [44]. Moreover, the slow rate of stiffness degradation in a ductile adhesive allows the redistribution of stresses within it, whereas in a brittle one, after the damage initiation, uncontrolled crack growth leads to a more catastrophic failure. In addition to this, the lower strength of a ductile adhesive is compensated for its higher fracture toughness.

Therefore, if the stress and strain fields are more advantageous for T-joints using ductile adhesive and, consequently, responsible for longer fatigue lives, the adhesion between adhesives and adherends, as well as the stiffness of the adherends, cannot be neglected in the fatigue resistance of the joints. In the first case, it is well documented in the literature that an adhesive joint with low adhesion strength between constituents can fail unpredictably and cause adhesive failure [53,54], which is clearly visible in this study for adhesive joints involving composite base plates (Figure 5a). The adhesive always adheres to the T-element, and the fatigue lives are much shorter than those observed in joints with aluminum base plates, as mentioned above. On the other hand, regarding the adhesive joints involving Al 6063-T5 base plates, Reis et al. [7] report that increasing the stiffness of the adherends promotes a more uniform distribution of stresses in the adhesive and the less stiff material determines the strength of the joint. In this context, and because the composite used in the base plate is less stiff (43.8 N/mm) than Al 6063-T5 (225.7 N/mm), it justifies the longer fatigue lives observed for these T-joints.

Finally, in terms of damage mechanisms observed for the cyclic loads, they were similar to those observed in the static response. Therefore, to avoid the repetition of images, the authors chose not to display them. Nevertheless, as can be seen in Figure 9 and for all the configurations studied, the crack started at the edge of the T-element and propagated towards its center with the application of the cyclic load due to the mixed-mode stress on the adhesive layer. The peeling stresses (σ_y) predominate over the smaller stresses τ_{xy} , whose distribution has peaks at both edges of the adhesive layer and which will be higher for the stiff adhesive. More detailed analysis also revealed that, in the T-joints involving composite base plates, the crack propagation occurred between the adhesive and the base plate due to the poor adhesive/composite adhesion strength, while in those involving Al 6063-T5 base plates, the failure mode was mixed (mixed adhesive/cohesive failure). In the latter case, and in places where cohesive failure occurs, the adhesion between adhesive/aluminum is very high and even exceeds the values of the applied load or the internal forces between the adhesive molecules [45].

In order to complement this damage analysis, the literature is consensual that residual stiffness is an adequate methodology to assess fatigue damage [41]. The damage initiation

and propagation cause changes in stiffness that can be monitored non-destructively, and for this purpose, the corresponding load and displacement values were also collected during the fatigue tests. Therefore, Figure 11 plots E/E_0 versus N/N_f , where E is the stiffness modulus (N/mm) at any given moment of the test, E_0 is the initial value of E (N/mm), N is the current number of cycles, and N_f is the number of cycles to failure. It is possible to observe that the damage accumulation previously discussed for all configurations can be corroborated by the global stiffness loss observed in Figure 11 and simultaneously confirms the findings of Sheno et al. [22]. However, the profile of the stiffness loss curves contradicts what is described in the literature [22] and shows to be very dependent on the applied load and materials involved in the T-joints (adhesives and adherends).

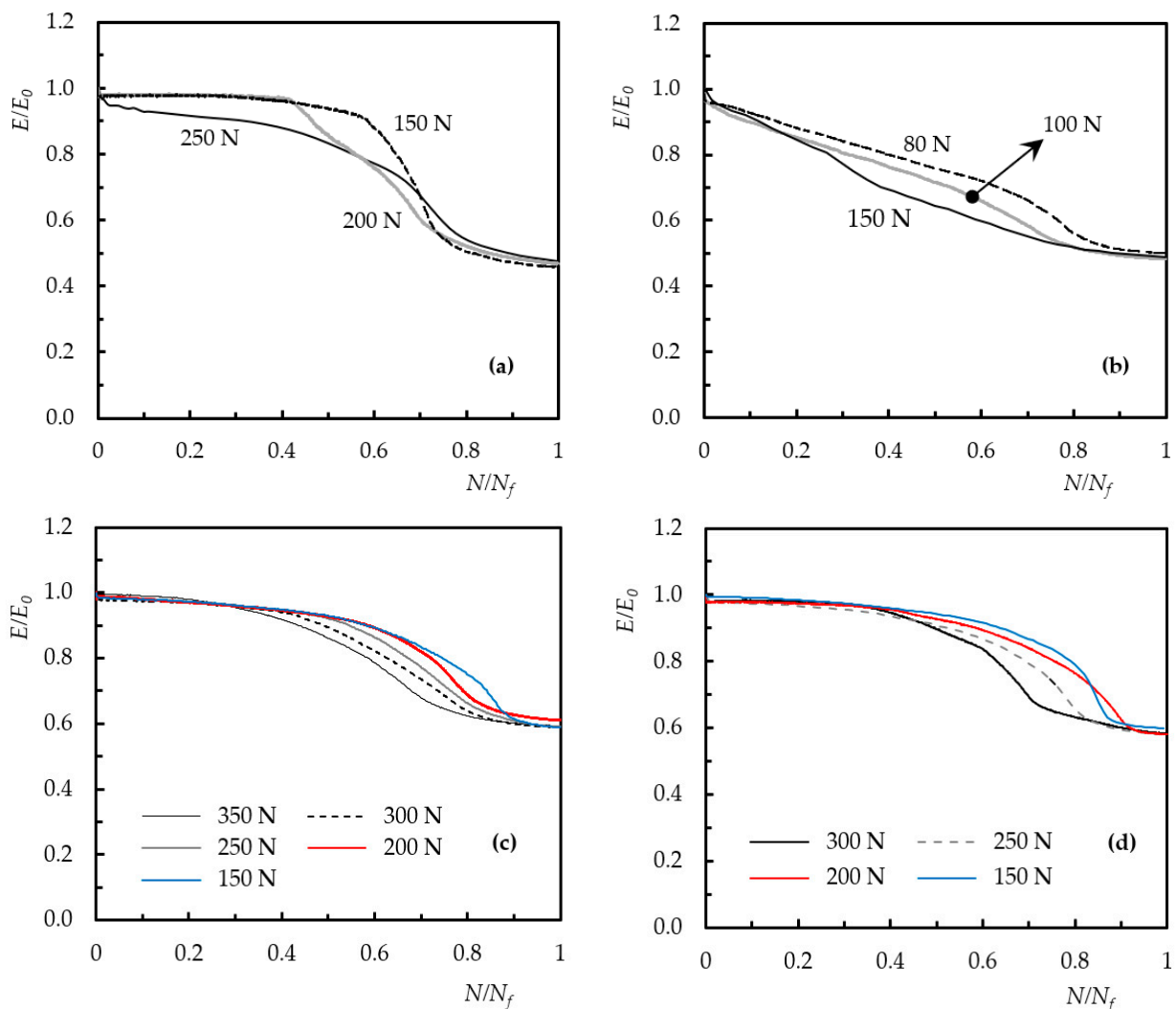


Figure 11. E/E_0 against the normalized number of cycles N/N_f for T-joints involving: (a) Composite base plate and ductile adhesive; (b) composite base plate and stiff adhesive; (c) Al 6063-T5 base plate and ductile adhesive; (d) Al 6063-T5 base plate and stiff adhesive.

In terms of T-joints involving composite base plates, for example, the stiff adhesive is responsible for curves in which the stiffness decreases almost linearly until about 60–70% of fatigue life, followed by a rapid degradation that culminates in a slower decrease until the adopted failure criterion is reached. These three regimes are repeated for the different load values, but the slope of the curve in the quasi-linear regime increases with increasing applied load. Therefore, this type of profile shows that the damage starts and propagates rapidly, leading to shorter lives. On the other hand, when these T-joints involve the ductile adhesive, the first regime is characterized by an almost unchanged stiffness (more or less

constant plateau) until a sharp loss of stiffness occurs, followed by a slower decrease until the adopted failure criterion is reached (third regime). It is noticeable that, for the lowest loads (200 N and 150 N), the second regime started between 40% and 60% of the fatigue life, while for the highest load (250 N), the curve is similar to those observed for the stiff adhesive. Therefore, longer primary regimes promote slower damage propagation and longer fatigue lives.

Finally, for T-joints involving the aluminum base plates, the curves show a very similar profile for both adhesives used and are characterized by three regimes similar to those observed for the lowest loads shown in Figure 4a. In this context, analogous to what was observed before, the extension of the primary regime is also a determining factor in fatigue life. For the stiff adhesive, it is around 40% of the fatigue life, while for the ductile one, it represents between 30% and 60% of the fatigue life. Subsequently, the second regime is smoother than that observed for the brittle adhesive, revealing slower damage propagation and, consequently, longer fatigue lives.

4. Conclusions

The main goal of this study was to analyze the damage mechanisms as well as the mechanical behavior of T-joints involving different adhesives and base plate materials. For this purpose, four configurations involving base plates of Al 6063-T5 and fiberglass composite with a T-element of Al 6063-T5 were studied, which were bonded with a stiff adhesive (Araldite® AV 4076-1/HY 4076) and a more ductile one (Araldite® AW 106/HV 953 U).

In terms of static response, load-displacement curve profiles common to all configurations were found, in which the load increases up to a certain value and, subsequently, decreases until it reaches the load-displacement curve of the respective base plate. This is explained by the initiation of a crack that begins at the edge of the T-element and propagates more or less rapidly into its interior, depending on the failure surface morphology. T-joints with aluminum base plates experienced mixed adhesive/cohesive failure, while those with composite base plates experienced an adhesive failure. Finally, after decreasing, the curves practically overlap those of the base plate material, reaching a new peak load that coincides with the maximum load obtained for the base plate material. Consequently, the first highest peak loads are obtained with the ductile adhesive (AW 106), where the values obtained for T-joints involving Al 6063-T5 base plates are 2.8 times higher than those involving composite base plates.

Regarding fatigue strength, for both base plate materials, it was observed that the ductile adhesive promotes higher fatigue lives due to higher elongation percentages before failure and lower stress concentrations. For example, the fatigue life of aluminum-based T-joints is around 871 and 3 times longer than that of joints using composite base plates and brittle and ductile adhesive, respectively. Finally, damage accumulation can be corroborated by the stiffness loss curves, where three regimes were found to exist. Longer first regimens and less abrupt second regimens promoted longer fatigue lives.

Author Contributions: Conceptualization, P.N.B.R. and J.A.M.F.; methodology, G.C.G.S. and P.N.B.R.; validation, G.C.G.S. and P.N.B.R.; formal analysis, G.C.G.S., J.A.M.F. and P.N.B.R.; investigation, G.C.G.S. and P.N.B.R.; data curation, G.C.G.S., J.A.M.F. and P.N.B.R.; writing—original draft preparation, G.C.G.S. and P.N.B.R.; writing—review and editing, P.N.B.R. and J.A.M.F. All authors have read and agreed to the published version of the manuscript.

Funding: This research received no external funding.

Data Availability Statement: Not applicable.

Acknowledgments: This research was sponsored by national funds through FCT—Fundação para a Ciência e a Tecnologia, under the project UIDB/00285/2020 and LA/P/0112/2020.

Conflicts of Interest: The authors declare no conflict of interest.

References

1. Ciardiello, R. The mechanical performance of re-bonded and healed adhesive joints activable through induction heating systems. *Materials* **2021**, *14*, 6351. [CrossRef]
2. Reis, P.N.B.; Antunes, F.J.V.; Ferreira, J.A.M. Influence of superposition length on mechanical resistance of single-lap adhesive joints. *Compos. Struct.* **2005**, *67*, 125–133. [CrossRef]
3. Da Silva, L.F.M.; Critchlow, G.W.; Figueiredo, M.A.V. Parametric study of adhesively bonded single lap joints by the Taguchi method. *J. Adhes. Sci. Technol.* **2008**, *22*, 1477–1494. [CrossRef]
4. Sawa, T.; Liu, J.; Nakano, K.; Tanaka, J.J. A two-dimensional stress analysis of single-lap adhesive joints of dissimilar adherends subjected to tensile loads. *J. Adhes. Sci. Technol.* **2000**, *14*, 43–66. [CrossRef]
5. Liu, J.; Sawa, T.; Toratani, H. A two-dimensional stress analysis and strength of single-lap adhesive joints of dissimilar adherends subjected to external bending moments. *J. Adhes.* **1999**, *69*, 263–291. [CrossRef]
6. Da Silva, L.F.M.; Carbas, R.J.C.; Critchlow, G.W.; Figueiredo, M.A.V.; Brown, K. Effect of material, geometry, surface treatment and environment on the shear strength of single lap joints. *Int. J. Adhes. Adhes.* **2009**, *29*, 621–632. [CrossRef]
7. Reis, P.N.B.; Ferreira, J.A.M.; Antunes, F. Effect of adherend's rigidity on the shear strength of single lap adhesive joints. *Int. J. Adhes. Adhes.* **2011**, *31*, 193–201. [CrossRef]
8. Amaro, A.M.; Neto, M.A.; Loureiro, A.; Reis, P.N.B. Taper's angle influence on the structural integrity of single-lap bonded joints. *Theor. Appl. Fract. Mech.* **2018**, *96*, 231–246. [CrossRef]
9. Sheno, R.A.; Read, P.J.C.L.; Hawkins, G.L. Fatigue failure mechanisms in fibre-reinforced plastic laminated tee joints. *Int. J. Fatigue* **1995**, *17*, 415–426. [CrossRef]
10. Johnson, N.L.; Kardomateas, G.A. Structural Adhesive Joints for Application to a Composite Space Frame—Analysis and Testing. *SAE Tech. Pap.* **1988**, 880892. [CrossRef]
11. Sheno, R.A.; Violette, F.L.M. A Study of Structural Composite Tee Joints in Small Boats. *J. Compos. Mater.* **1990**, *24*, 644–666. [CrossRef]
12. Moreno, M.C.S.; Cela, J.J.L.; Vicente, J.L.M.; Vecino, J.A.G. Adhesively bonded joints as a dissipative energy mechanism under impact loading. *Appl. Math. Model.* **2015**, *39*, 3496–3505. [CrossRef]
13. Li, W.; Blunt, L.; Stout, K.J. Analysis and design of adhesive-bonded tee joints. *Int. J. Adhes. Adhes.* **1997**, *17*, 303–311. [CrossRef]
14. Li, W.; Blunt, L.; Stout, K.J. Stiffness analysis of adhesive bonded Tee joints. *Int. J. Adhes. Adhes.* **1999**, *19*, 315–320. [CrossRef]
15. Apalak, Z.G.; Apalak, M.K.; Davies, R. Analysis and design of adhesively bonded tee joints with a single support plus angled reinforcement. *J. Adhes. Sci. Technol.* **1996**, *10*, 681–724. [CrossRef]
16. Apalak, Z.G.; Apalak, M.K.; Davies, R. Analysis and design of tee joints with double support. *Int. J. Adhes. Adhes.* **1996**, *16*, 187–214. [CrossRef]
17. Sheno, R.A.; Hawkins, G.L. Influence of material and geometry variations on the behaviour of bonded tee connections in FRP ships. *Composites* **1992**, *23*, 335–345. [CrossRef]
18. Dodkins, A.R.; Sheno, R.A.; Hawkins, G.L. Design of Joints and Attachments in FRP Ships' Structures. *Mar. Struct.* **1994**, *7*, 365–398. [CrossRef]
19. Sheno, R.A.; Read, P.J.C.L.; Jackson, C.L. Influence of joint geometry and load regimes on sandwich tee joint behaviour. *J. Reinf. Plast. Compos.* **1998**, *17*, 725–740. [CrossRef]
20. Crocker, L.E.; Gower, M.R.L.; Broughton, W.R. Finite Element Assessment of Geometric and Material Property Effects on the Strength and Stiffness of Bonded and Bolted T-Joints. NPL Report MATC(A)124. 2003. Available online: <https://eprintspublications.npl.co.uk/2563/> (accessed on 9 July 2023).
21. Chaves, F.J.P.; da Silva, L.F.M.; de Castro, P.M.S.T. Adhesively bonded T-joints in polyvinyl chloride windows. *Proc. Inst. Mech. Eng. Part L J. Mater. Des. Appl.* **2008**, *222*, 159–174. [CrossRef]
22. Zhan, X.; Gu, C.; Wu, H.; Liu, H.; Chen, J.; Chen, J.; Wei, Y. Experimental and numerical analysis on the strength of 2060 Al–Li alloy adhesively bonded T joints. *Int. J. Adhes. Adhes.* **2016**, *65*, 79–87. [CrossRef]
23. Ferreira, J.A.M.; Campilho, R.D.S.G.; Cardoso, M.G.; Silva, F.J.G. Numerical simulation of adhesively-bonded T-stiffeners by cohesive zone models. *Procedia Manuf.* **2020**, *51*, 870–877. [CrossRef]
24. Ma, X.; Bian, K.; Liu, H.; Wang, Y.; Xiong, K. Numerical and experimental investigation of the interface properties and failure strength of CFRP T-Stiffeners subjected to pull-off load. *Mater. Des.* **2020**, *185*, 108231. [CrossRef]
25. Ravindran, A.R.; Ladani, R.B.; Wang, C.H.; Mouritz, A.P. Strengthening of composite T-joints using 1D and 2D carbon nanoparticles. *Compos. Struct.* **2021**, *255*, 112982. [CrossRef]
26. Carvalho, P.M.D.; Campilho, R.D.S.G.; Sánchez-Arce, I.J.; Rocha, R.J.B.; Soares, A.R.F. Adhesively-bonded T-joint cohesive zone analysis using dual-adhesives. *Procedia Struct. Integr.* **2022**, *41*, 24–35. [CrossRef]
27. Morano, C.; Wagih, A.; Alfano, M.; Lubineau, G. Improving performance of composite/metal T-joints by using corrugated aluminum stiffeners. *Compos. Struct.* **2023**, *307*, 116652. [CrossRef]
28. Read, P.J.C.L.; Sheno, R.A. Fatigue behaviour of single skin FRP tee joints. *Int. J. Fatigue* **1999**, *21*, 281–296. [CrossRef]
29. Marcadon, V.; Nadot, Y.; Roy, A.; Gacougnolle, J.L. Fatigue behaviour of T-joints for marine applications. *Int. J. Adhes. Adhes.* **2006**, *26*, 481–489. [CrossRef]
30. Loureiro, L.; da Silva, L.F.M.; Sato, C.; Figueiredo, M.A.V. Comparison of the mechanical behaviour between stiff and flexible adhesive joints for the automotive industry. *J. Adhes.* **2010**, *86*, 765–787. [CrossRef]

31. Cullinan, J.F.; Velut, P.; Michaud, V.; Wisnom, M.R.; Bond, I.P. In-situ repair of composite sandwich structures using cyanoacrylates. *Compos. Part A Appl. Sci. Manuf.* **2016**, *87*, 203–211. [[CrossRef](#)]
32. Almaraz, G.M.D.; Ambriz, J.L.A.; Calderón, E.C. Fatigue endurance and crack propagation under rotating bending fatigue tests on aluminum alloy AISI 6063-T5 with controlled corrosion attack. *Eng. Fract. Mech.* **2012**, *93*, 119–131. [[CrossRef](#)]
33. Santos, P.S.; Maceiras, A.; Valvez, S.; Reis, P.N.B. Mechanical characterization of different epoxy resins enhanced with carbon nanofibers. *Frat. Ed. Integrità Strutt.* **2020**, *15*, 198–212. [[CrossRef](#)]
34. Negru, R.; Marsavina, L.; Hluscu, M. Experimental and Numerical Investigations on Adhesively Bonded Joints. *IOP Conf. Ser. Mater. Sci. Eng.* **2016**, *123*, 012012. [[CrossRef](#)]
35. Mitchell, A.J. The Optimization of Stress Transfer Characteristics in Adhesively Bonded Vehicular Armour by Modification of the Adhesive Phase and by Engineering the Adhesive-to-Metal and Adhesive-to-Composite Interphases. Ph.D. Thesis, Loughborough University, Loughborough, UK, 2016.
36. Pereira, A.M.; Reis, P.N.B.; Ferreira, J.A.M.; Antunes, F.V. Effect of saline environment on mechanical properties of adhesive joints. *Int. J. Adhes. Adhes.* **2013**, *47*, 99–104. [[CrossRef](#)]
37. Reis, P.N.B.; Monteiro, J.F.R.; Pereira, A.M.; Ferreira, J.A.M.; Costa, J.D.M. Fatigue behaviour of epoxy-steel single lap joints under variable frequency. *Int. J. Adhes. Adhes.* **2015**, *63*, 66–73. [[CrossRef](#)]
38. Reis, P.N.B.; Pereira, A.M.; Ferreira, J.A.M.; Costa, J.D.M. Cyclic creep response of adhesively bonded steel lap joints. *J. Adhes.* **2017**, *93*, 704–715. [[CrossRef](#)]
39. Pereira, A.M.; Reis, P.N.B.; Ferreira, J.A.M. Effect of the mean stress on the fatigue behaviour of single lap joints. *J. Adhes.* **2017**, *93*, 504–513. [[CrossRef](#)]
40. Ferreira, J.A.M.; Reis, P.N.B.; Costa, J.D.M.; Richardson, M.O.W. Fatigue behaviour of composite adhesive lap joints. *Compos. Sci. Technol.* **2002**, *62*, 1373–1379. [[CrossRef](#)]
41. Reis, P.N.B.; Ferreira, J.A.M.; Richardson, M.O.W. Effect of the surface preparation on PP reinforced glass fiber adhesive lap joints strength. *J. Thermoplast. Compos. Mater.* **2012**, *25*, 3–11. [[CrossRef](#)]
42. Serra, G.C.G.; Reis, P.N.B.; Ferreira, J.A.M. Effect of cure temperature on the mechanical properties of epoxy-aluminium single lap joints. *J. Adhes.* **2023**, *99*, 1441–1455. [[CrossRef](#)]
43. Akhavan-Safar, A.; Ramezani, F.; Delzendehrooy, F.; Ayatollahi, M.R.; da Silva, L.F.M. A review on bi-adhesive joints: Benefits and challenges. *Int. J. Adhes. Adhes.* **2022**, *114*, 103098. [[CrossRef](#)]
44. Kadioglu, F.; Adams, R. Non-linear analysis of a ductile adhesive in the single lap joint under tensile loading. *J. Reinf. Plast. Compos.* **2009**, *28*, 2831–2838. [[CrossRef](#)]
45. Da Silva, L.F.M.; Neves, P.J.C.; Adams, R.D.; Wang, A.; Spelt, J.K. Analytical Models of Adhesively Bonded Joints—Part II: Comparative Study. *Int. J. Adhes. Adhes.* **2009**, *29*, 331–341. [[CrossRef](#)]
46. Ciardiello, R.; Niutta, C.B.; Goglio, L. Adhesive thickness and ageing effects on the mechanical behaviour of similar and dissimilar single lap joints used in the automotive industry. *Processes* **2023**, *11*, 433. [[CrossRef](#)]
47. Hirulkar, N.S.; Jaiswal, P.R.; Reis, P.N.B.; Ferreira, J.A.M. Bending strength of single-lap adhesive joints under hygrothermal aging combined with cyclic thermal shocks. *J. Adhes.* **2021**, *97*, 493–507. [[CrossRef](#)]
48. Da Silva, L.F.M.; Pirondi, A.; Öchsner, A. *Hybrid Adhesive Joints*; Springer: Berlin/Heidelberg, Germany; London, UK, 2011; p. 304.
49. Barbosa, N.G.C.; Campilho, R.D.S.G.; Silva, F.J.G.; Moreira, R.D.F. Comparison of different adhesively-bonded joint types for mechanical structures. *Appl. Adhes. Sci.* **2018**, *6*, 15. [[CrossRef](#)]
50. Karachalios, E.F.; Adams, R.D.; da Silva, L.F.M. The behaviour of single lap joints under bending loading. *J. Adhes. Sci. Technol.* **2013**, *27*, 1811–1827. [[CrossRef](#)]
51. Meredith, H.J.; Wilker, J.J. The interplay of modulus, strength, and ductility in adhesive design using biomimetic polymer chemistry. *Adv. Funct. Mater.* **2015**, *25*, 5057–5065. [[CrossRef](#)]
52. Temiz, Ş. Application of bi-adhesive in double-strap joints subjected to bending moment. *J. Adhes. Sci. Technol.* **2006**, *20*, 1547–1560. [[CrossRef](#)]
53. De Barros, S.; Kenedi, P.P.; Ferreira, S.M.; Budhe, S.; Bernardino, A.J.; Souza, L.F.G. Influence of mechanical surface treatment on fatigue life of bonded joints. *J. Adhes.* **2017**, *93*, 599–612. [[CrossRef](#)]
54. Pereira, A.M.; Ferreira, J.M.; Antunes, F.V.; Bártolo, P.J. Study on the fatigue strength of AA 6082-T6 adhesive lap joints. *Int. J. Adhes. Adhes.* **2009**, *29*, 633–638. [[CrossRef](#)]

Disclaimer/Publisher’s Note: The statements, opinions and data contained in all publications are solely those of the individual author(s) and contributor(s) and not of MDPI and/or the editor(s). MDPI and/or the editor(s) disclaim responsibility for any injury to people or property resulting from any ideas, methods, instructions or products referred to in the content.